

Erosional unloading, hillslope geometry, and the height of the Cascade Range, Washington State, USA

Sara Mitchell,^{1*} David Montgomery² and Harvey Greenberg²

¹ Biology Department, College of the Holy Cross, Worcester, MA, USA

² Earth and Space Sciences, University of Washington, Seattle, WA, USA

Received 15 July 2008; Revised 9 January 2009; Accepted 19 January 2009

* Correspondence to: Sara Mitchell, Biology Department, College of the Holy Cross, 1 College Street, Worcester, MA 01610, USA. E-mail: smitchel@holycross.edu

ESPL

Earth Surface Processes and Landforms

ABSTRACT: Peaks in the Cascade Range in northern Washington State are on average ~800 m higher than in southern Washington. The influences of differential valley excavation and variations in hillslope length and average slope on these altitudinal trends were tested using a 3-dimensional model for isostatic rock uplift and calculations of hillslope length and slope respectively. The magnitude of isostatic peak uplift calculated by the model is highly dependent on the flexural rigidity (D) and the related effective elastic thickness (T_e) of the crust of this region. Crustal rigidity was constrained using published estimates and by estimating the depth of the seismogenic zone in the area ($D > 1 \times 10^{23}$ Nm and $T_e > 24$ km). With these constraints, isostatic compensation due to differential erosion added < 700 m and 300 m, or < 25% overall, of height to peaks in the northern and southern Cascades, respectively. Deeper valley incision in the northern Cascades accounts for < 300 m of the 800 m difference in peak altitudes between north and south. Similarly, variation in valley spacing and slope account for < 350 m of the difference in mean altitude between northern and southern regions. Hence, at least several hundred m difference in altitude between the northern and southern regions of the Cascades in Washington must be due to tectonic, geologic, or geophysical factors rather than surficial and geomorphic effects like isostatic response to valley incision and hillslope geometry. Copyright © 2009 John Wiley & Sons, Ltd.

KEYWORDS: isostasy; uplift; topography; GIS; Cascade Range

Introduction

How valley incision and the creation of relief influence the peak altitudes of mountain ranges has been a topic of considerable interest over the past several decades (e.g. Molnar and England, 1990; Gilchrist *et al.*, 1994; Montgomery, 1994; Small and Anderson, 1998; Whipple *et al.*, 1999; Montgomery and Greenberg, 2000). Incision of valleys at rates higher than the erosion of adjacent peaks causes spatially non-uniform unloading which, when isostatically compensated at depth, causes peaks to rise by some amount (Wager, 1933; Holmes, 1945). Molnar and England (1990) hypothesized a feedback system wherein increased valley incision brought on by global cooling and enhanced glacial erosion could effectively raise the crests of mountain ranges, thereby influencing local and global climate patterns and further enhance range development. However, because the volume of crust removed is replaced by a smaller volume of denser mantle, the average altitude of the area will be lower than it was originally (Holmes, 1945; Molnar and England, 1990). The influence of this feedback is limited by how much altitude neighboring peaks can realistically gain via valley incision.

In this study, we determine the maximum extent to which differences in isostatic compensation from relief creation

contribute to the south-to-north increase in peak altitudes in the Cascade Range of Washington State. We also consider geomorphic parameters including slope and valley spacing as potential controls on range-scale altitude trends. Constraining the degree to which geology, tectonics, and crustal thickness individually contribute to altitude trends was beyond the scope of this investigation.

Rigidity of the lithosphere

The uplift of peaks resulting from the isostatic response to valley incision [from here on referred to as 'superelevation,' following Montgomery and Greenberg (2000)] is a function of the flexural strength of the lithosphere in that location (Turcotte and Schubert, 1982); however, the strength of the lithosphere in geologically and tectonically complex regions such as orogenic belts and subduction zones is difficult to estimate independently (Miller and Paterson, 2001; Lowry *et al.*, 2000; Flück *et al.*, 2003; Burov and Watts, 2006). In this investigation, we used several estimates for effective elastic thickness and/or flexural rigidity to constrain the maximum possible isostatic response of the Cascade landscape to relief creation, and thus the degree to which this

Table 1. List of symbols

T_e	Effective elastic thickness (km)
D	Flexural rigidity (N m)
E	Modulus of elasticity (8.35×10^{10} N m ⁻²)
ν	Poisson's ratio (0.25)
Nm	Newton-meters
w	"Superelevation," vertical deflection of the landscape due to rebound
ρ/α	Non-dimensional distance from point load
α	Flexural rigidity parameter
z	Equivalent eroded thickness (m)
q	Point load used in isostasy calculation
π	3.1415
ρ_m	Density of the mantle (3300 kg/m ³)
ρ_c	Density of the crust (2800 kg/m ³)
g	Acceleration due to gravity (9.81 m s ⁻²)
Kei	Kelvin function
dx, dy	Grid cell dimensions (m)
M	Earthquake magnitude
l_s	Hillslope length (m)
\bar{l}_s	Mean hillslope length (m)
D_d	Drainage density
θ	Slope angle
\bar{Z}_m	Mean altitude above valley floor (m)
ΔZ_m	Difference in mean altitude above valley floor (m)
V_p	P-wave velocity
V_s	S-wave velocity

response could contribute to the general altitude trends of the range.

The strength of the lithosphere is generally expressed either in terms of flexural rigidity (D) or effective elastic thickness (T_e), which relate to each other by:

$$D = \frac{ET_e^3}{12(1-\nu^2)} \quad (1)$$

where E is the modulus of elasticity (8.35×10^{10} N m⁻²) and ν is Poisson's ratio (0.25) (list of symbols in Table 1). Although valley incision can be constrained using geographic information system (GIS) techniques, and the densities of the crust and mantle can be estimated with reasonable accuracy, it remains difficult to constrain the strength of the crust (Burov and Watts, 2006). While Airy isostasy, a hypothetical condition in which the crust has no strength and isostatic effects are purely local, is often used as an endmember in uplift calculations (e.g. Small and Anderson, 1998; Montgomery and Greenberg, 2000), uncertainty remains in constraining a realistic lithospheric strength.

The value of T_e is highly variable in continental settings, ranging between 0 and 100 km depending on the age, temperature, and thickness of the lithosphere (Burov and Watts, 2006), as well as the timescale of deformation (Thatcher and Pollitz, 2008). Many techniques have been used to estimate T_e (and thus D) for different tectonic and lithospheric environments. Maggi *et al.* (2000), for example, argued that the primary strength was contained within the brittle seismogenic zone, and thus the thickness of the seismogenic zone (T_s) is equivalent to T_e . Adopting this logic, one may constrain T_e through earthquake focal depths. In contrast, Watts and Burov (2003) argued that T_e should instead represent the combined brittle, ductile, and elastic strength of the lithosphere and therefore $T_s < T_e$ in most continental settings. Constraints on T_e are also estimated via modeling from topography and Bouguer anomalies (e.g. Flück *et al.*, 2003; Perez-Gussinye *et al.*, 2004) and thermomechanical and viscoelastic properties (Burov and Watts, 2006; Cohen and Darby, 2003). Other T_e estimates come from measured deformation resulting from

glacial unloading, though the estimates derived from phenomena with 10^4 – 10^5 timescales may not apply over the longer timescales relevant to erosional unloading (e.g. James *et al.*, 2000; Thatcher and Pollitz, 2008).

Nearly all previous studies on peak uplift due to valley incision acknowledge the importance of constraining D or T_e and the resulting uncertainty in the uplift calculations. Montgomery (1994) estimated the maximum peak uplift of the Himalaya, Sierra Nevada, and Tibetan Plateau assuming purely local (Airy) isostatic compensation, and then assessed the percentage of local (maximum) compensation that would occur given a range of D from 10^{20} to 10^{25} N m. Gilchrist *et al.* (1994) acknowledged that their estimate for uplift of the European Alps based on Airy isostasy by definition provides a maximum constraint. Small and Anderson (1998) estimated isostatic uplift of Laramide mountain ranges to be ~290 m using Airy isostasy, but ~90 m using a minimum plausible T_e estimate of 16 km. Montgomery and Greenberg (2000) similarly use a range of T_e of 5 to 24 km to calculate ~500–700 m of superelevation in the Olympic Mountains of Washington State. Pelletier (2004) uses a three-dimensional model based on the flexure equation (Watts, 2001) to determine ratios of rock uplift to erosion resulting from glacial erosion in mountain ranges of the western United States, including the Cascades. Pelletier's model takes into account spatial variability in lithospheric rigidity; however, it assumes spatially uniform erosion in glaciated areas and thus does not specifically solve for peak superelevation resulting from relief creation, as we do here. Stern *et al.* (2005) used isostasy to constrain the rheology of the Transantarctic Mountains. They modeled the isostatic uplift of the range using four different rheological models and identified the flexural rigidity that resulted in uplift that best fit observed deformation of erosion surfaces. Using this model, they showed that isostasy may account for 25% of the total peak altitude of the Transantarctic Mountains, a percentage comparable to those reported in other areas (Montgomery, 1994; Gilchrist *et al.*, 1994). Recently, Medvedev *et al.* (2008) used a numerical model of isostatic rebound and a T_e of 20 km to suggest that >1 km of vertical rock uplift has occurred in Greenland as a result of compensation from glacial erosion.

Study area

We used the techniques of Montgomery and Greenberg (2000) to investigate the effects of valley incision on the topography of the Cascade Range in Washington State. The Cascade Range forms a 150- to 220-km-wide topographic high that bisects the state from south to north (Figure 1). Although recent subduction arc volcanism has created five large and currently active stratovolcanoes, the range itself is an antiform and many of the peaks in the range, particularly in the north, consist of uplifted sedimentary rocks and exhumed plutonic and metamorphic rocks (Schuster, 2005). While the 'Cascade Range' as a physiographic entity extends many hundreds of kilometers through Oregon and south to California, we use the phrase 'North Cascades' to refer to the range located north of the Snoqualmie and Yakima Rivers to the Canadian border; the term 'southern Cascades' refers to the range south to the Washington-Oregon border (Figure 1A). We chose this boundary because previous work has suggested that the Cascade Range experienced significantly different geologic, tectonic, and thus geomorphic histories in these two regions of the Cascades. According to the interpretations of Mackin and Cary (1965) and Mitchell and Montgomery (2006a), the North Cascades existed as high topography prior to the middle Miocene, whereas the southern Cascades were uplifted from low altitude

after the middle Miocene. In central Washington, Quaternary glacial erosion removed rock preferentially at and above the Quaternary average glacial equilibrium line altitude (ELA) independent of large west–east gradients in rock uplift rate, thereby masking major differences in mountain building history between the Cascades in northern and southern Washington (Mitchell and Montgomery, 2006b).

The primary tectonic feature of the Cascade region is the Cascadia subduction zone, located ~100 km west of the Washington coast and ~300 km west of the Cascades (Figure 2). Additional tectonic forcing is due to rotation of the Basin

and Range province to the south and east (e.g. England and Wells, 1991). The complex relationships between the converging and overlapping plates, rotational motion and extension, and active volcanic arc make it difficult to unravel the magnitude of tectonic forcing on the overall surface and rock uplift of the Cascade Range (Mitchell and Montgomery, 2006a). In this paper, we focus exclusively on the role of erosion-driven isostatic peak uplift and morphometric parameters, rather than all possible components, on range-spanning altitude trends.

We model the spatial distribution of superelevation using a range of flexural rigidities. Using independent constraints on

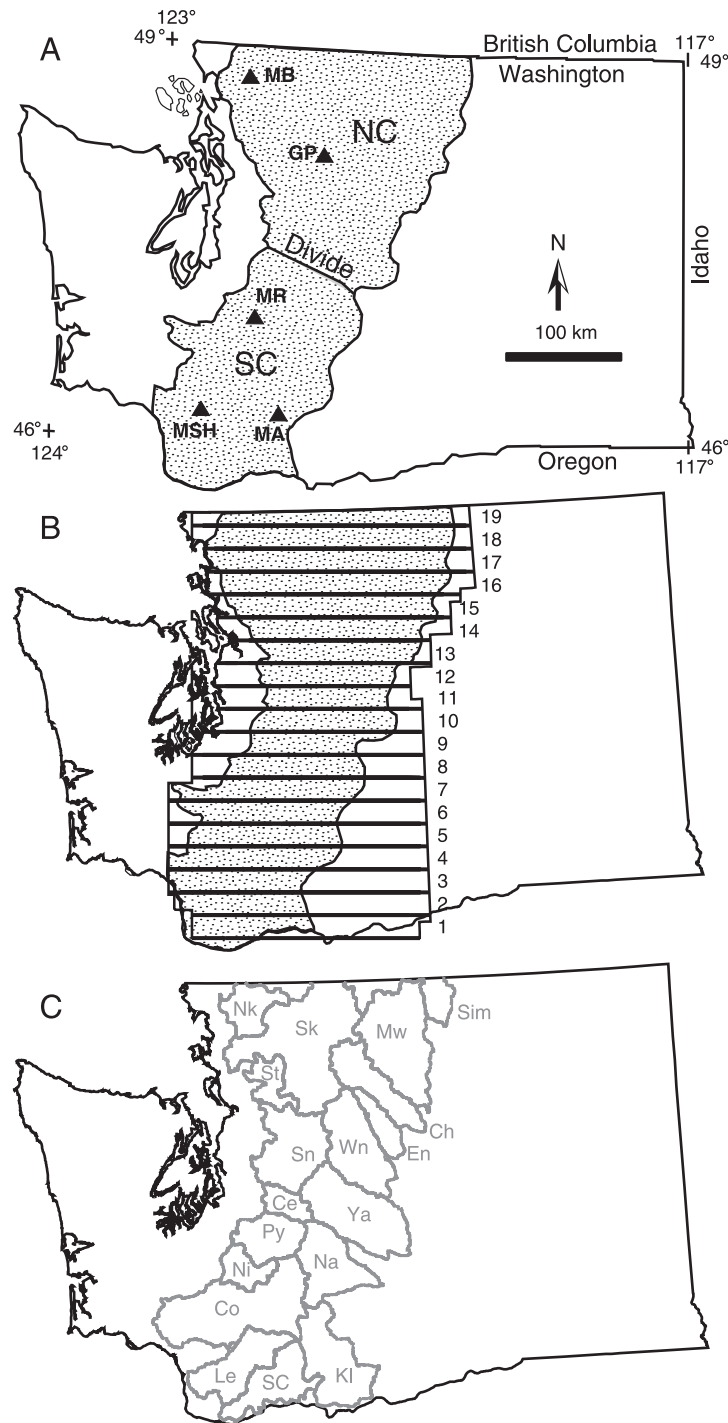


Figure 1. (A) Location of Cascade Range (stippled region) and Quaternary volcanoes (filled triangles) in Washington State. North Cascades = NC, southern Cascades = SC; Divide is the division between north and south, formed by the Snoqualmie and Yakima Rivers. Quaternary volcanoes are: MB, Mount Baker; GP, Glacier Peak; MR, Mount Rainier; MA, Mount Adams; MSH, Mount St Helens. (B) Location of analysis swaths (horizontal bars) numbered 1–19. (C) Location of drainage basins: Sim, Similkameen; Nk, Nooksack; Sk, Skagit; Mw, Methow; St, Stilliguamish; Ch, Chelan; En, Entiat; Wn, Wenatchee; Sn, Snoqualmie; Ce, Cedar-Green; Ya, Yakima; Py, Puyallup; Na, Naches; Ni, Nisqually; Co, Cowlitz; Kl, Klickitat; Le, Lewis; SC, South Columbia. Drainage basin characteristics are shown in Table III.

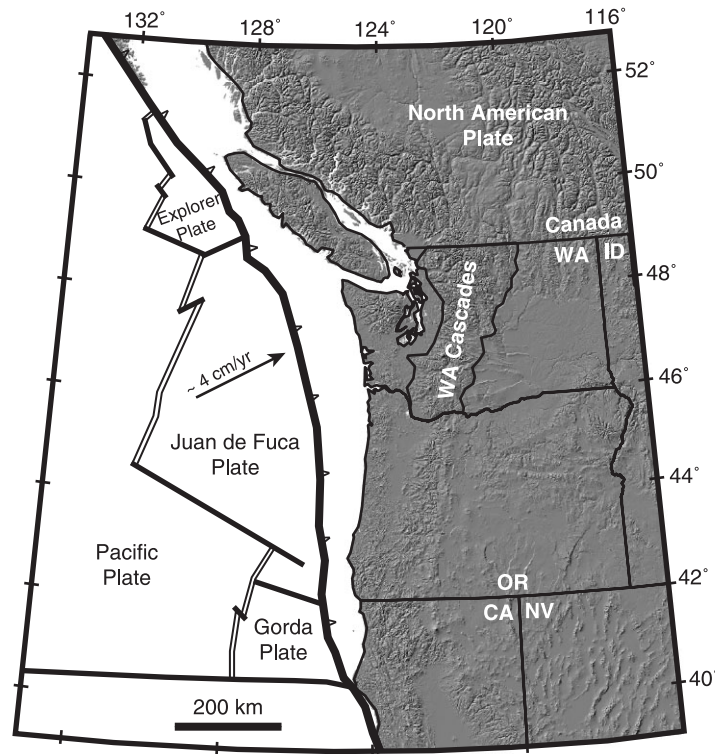


Figure 2. Tectonic map of the Pacific Northwest.

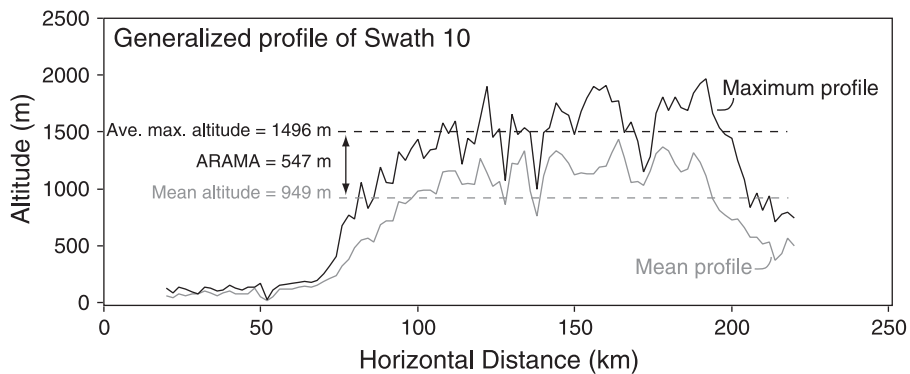


Figure 3. Illustration of average maximum altitude and ARAMA calculations. The profile is generalized from the topography of Swath 10 (Figure 1B). ARAMA is equal to the difference between the average maximum altitude and the mean altitude.

D, we then determine the maximum possible elevation that the Cascades could have gained through this process, and the degree to which isostatic effects cause north–south differences in the altitude of the range. Because peak uplift due to valley incision should reduce mean altitudes in areas undergoing the most incision and greatest peak uplift, we also explore the extent to which systematic variation in the topographic parameters of slope and valley spacing contribute to spatial variation in mean altitudes of the range.

Methods

We use GIS techniques to analyze topographic trends of the Cascade Range, quantify potential isostatic effects from valley incision, and constrain the role of valley spacing and slope on range-scale altitudinal gradients. All GIS work was conducted using a 10-m-grid-size digital elevation model (DEM) of the Cascade physiographic province and surrounding area, as defined by Haugerud (2004). The base DEM was constructed

by merging DEMs made from digitization of 7.5-minute USGS topographic quadrangles, and projection into Universal Transverse Mercator (UTM) Zone 10 coordinates. The vertical resolution of the DEM is 0.1 m.

Mean and maximum altitude

We analyzed large-scale, north–south trends in mean and maximum altitude by dividing the DEM of the Cascade physiographic province into 19 20-km wide, west–east trending ‘swaths’ (Figure 1B). Within each topographic swath, we calculated mean and maximum altitude at 10-m longitudinal (UTM Easting) intervals. We then determined the average of all the mean and maximum altitudes for each swath to get a metric representative of the overall peak altitude (Figure 3). Note that the ‘average maximum altitude’ is not the average of all summit altitudes; rather, it is the average of all the maximum altitudes projected across a 20-km swath of topography. Because the high-altitude Quaternary volcanoes

significantly inflate average maximum altitude values, yet are not relevant to isostatic calculations, we excluded the volcanoes from these calculations.

Range-scale trends in mean altitudes are influenced by a variety of factors unrelated to isostatic compensation or valley-ridge spacing, including inhomogeneity in fluvial baselevel elevations, crustal thickness, active tectonic uplift, or mantle temperature (Hasterok and Chapman, 2007; Turcotte and Schubert, 1982). For instance, the development of the same degree of relief on a high and a low plateau should create the same peak superelevation and lowering of mean elevations (all else being equal), but the absolute mean and peak altitudes on the high plateau will be higher simply because the original plateau was higher. Furthermore, valley incision will decrease the mean elevation of an area as it lifts peaks. Therefore, we determined a metric that removes the trend in mean altitudes from the north–south trend in maximum altitude. To isolate that part of the maximum elevation trend that may possibly be a function of isostatic compensation, we subtracted mean altitudes from the average of all maximum altitudes in each swath, clipped to the boundaries of the mountain range (Figure 3). This metric can be thought of as the swath-average half-relief, or relief above the mean altitude. We refer to this swath-averaged metric as the ARAMA, for ‘average relief above mean altitude.’

Finally, we determined the altitude of the five highest non-volcanic peaks in each swath. We use these peak altitudes to determine what percentage of the maximum height of the range (excluding volcanoes) can be attributed to superelevation.

Isostatic compensation

Using the three-dimensional rebound model of Montgomery and Greenberg (2000), we calculated the potential peak altitude gained from the creation of relief in the Cascades. We first determined the magnitude and spatial distribution of ‘missing mass’ below the peaks and ridges in the range, and then calculated the amount of isostatic uplift resulting from the mantle replacing that missing mass by summing the flexural response for the resulting negative load at each grid point. This method does not seek to reconstruct a realistic ‘pre-incision’ topography, nor does it account for potential differences in long-term exhumation that removes mass from both peaks and valleys.

To create a grid of missing mass, we chose an analysis window that contains the Cascades physiographic province in Washington State, plus a 100 km buffer to the north to remove edge effects of the uplift calculation. This buffer was not extended to the south across the Columbia River gorge. We then compiled a 90-m-grid-size DEM for this region using a resampled 10-m DEM, bathymetric data for Puget Sound, and DTED 3-arc-second data for Canada. Next, we located each peak (local maximum) within a 6.6 km radius. This 6.6 km radius was shown to be a length scale large enough to span major valleys but small enough not to exclude many mountain peaks of the nearby Olympic Mountains (Montgomery and Greenberg, 2000). This data set of peaks was then used to create a triangular irregular network (TIN) of 5428 local maxima, creating a reference surface similar to a rubber sheet connecting the highest peaks. The Quaternary volcanoes were removed from this surface, assigning the areas within 15 km of the summit of each large volcano the average elevation of points located in an annulus covering the area between 15 and 25 km from the summit. Then we subtracted the modern elevations from the 90-m DEM from this surface to create a grid showing

the thickness of ‘missing’ rock from below the reference surface for each cell.

Using this grid of missing rock mass, we calculated the vertical deflection resulting from the unloading (or loading, in the areas of the Quaternary volcanoes which add mass to the crust) of each grid cell (w) according to Lambeck (1988):

$$w\left(\frac{r}{\alpha}\right) = \left(\frac{q}{2\pi\rho_m g\alpha^2}\right) \text{Kei}\left(\frac{r}{\alpha}\right) \quad (2)$$

where (r/α) is the non-dimensional distance from the point load, g is the acceleration due to gravity (9.81 m s^{-2}), ρ_m is the density of the mantle (3300 kg m^{-3}), and Kei is a Kelvin function (Abramowitz and Stegun, 1964). The flexural rigidity parameter α is given by:

$$\alpha = (D/\rho_c g)^{1/4} \quad (3)$$

where D is the flexural rigidity (see Equation 1) and ρ_c is the density of the crust (2800 kg m^{-3}). Finally, q is the point load:

$$q = zg\rho_c dx dy \quad (4)$$

where z is the ‘missing’ thickness and dx and dy are the grid cell dimensions (90 m by 90 m). The overall vertical movement at any given point is affected by the amount of mass either lost or gained at that point and at all points near enough to also affect it. The flexural rigidity controls how far out and to what extent neighboring cells affect the uplift of each cell. We calculated w for each cell using the range of D observed in continental crust: from 10^{19} to 10^{24} N m (Burov and Watts, 2006).

While we used a full five-order-of-magnitude range of rigidities in the three-dimensional model for the Cascades, there are independent regional constraints for T_e (and thus D). For example, James *et al.* (2000) used post-glacial isostatic rebound rates to constrain the T_e of the Puget Lowland, adjacent to the northern Cascade region, to be between 30 and 40 km, equivalent to $D = 2.0$ to 4.8×10^{23} N m. Clague and James (2002) use similar methods to show that $T_e \sim 35$ km ($D \sim 3.2 \times 10^{23}$ N m) along the British Columbia coast, a few tens of kilometers northwest of the Cascades in Washington.

Because the depth of the seismogenic zone (T_s) for an area may also provide a minimum constraint on T_e (e.g. Maggi *et al.*, 2000; Watts and Burov, 2003), we estimated T_s using earthquake data retrieved from the Pacific Northwest Seismograph Network (PNSN), a service run by the Advanced National Seismic System run by the Northern California Earthquake Data Center (<http://www.ncedc.org/anss/catalog-search.html>, March 2006). These data include the date, magnitude, focus location, and focus depth for earthquakes occurring between 125° W and 117° W longitude, 45° N and 49° N latitude and happening between 1970 and 2006 (Figure 4). The PNSN employs the location algorithm of Hermann (1979), which uses simple one-dimensional p-velocity models with station corrections and a fixed V_p/V_s ratio of 1.78 to determine earthquake locations. Depths are determined using regional velocity models that incorporate the spatial distribution of stations and the underlying geology (R. Hartog, personal communication, 2008). Over 4300 earthquakes of magnitude (M) ≥ 2 occurred in this region and time period. Over 20 000 additional smaller earthquakes ($1 < M < 2$) occurred during this time; we did not include these in Figure 3 because their spatial distribution and depth were similar to those with $M > 2$. While T_e interpreted from the earthquake foci is complex due to the presence of the subducting slab of the Juan de Fuca plate, the T_e estimated from the depth of the seismogenic zone on

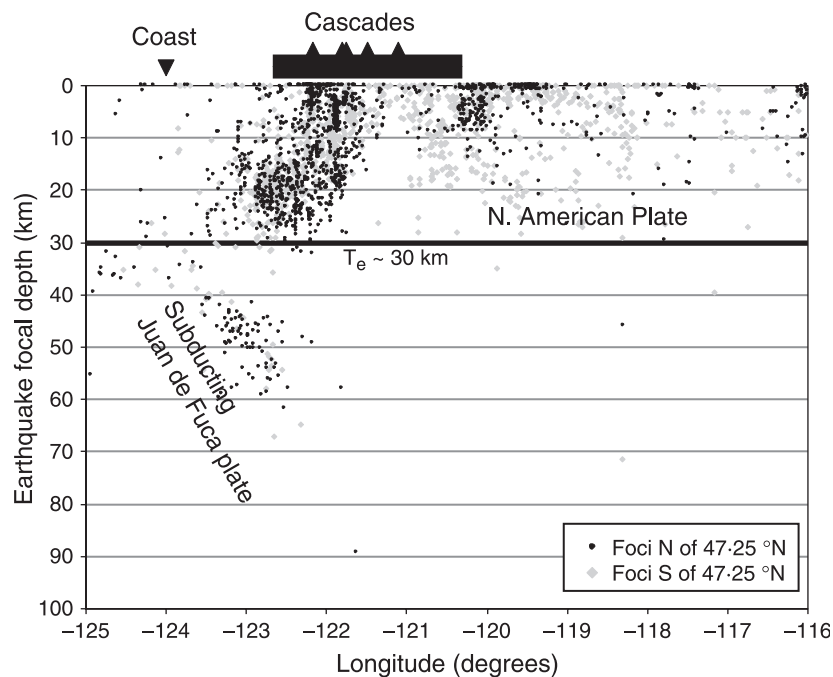


Figure 4. $M > 2$ Earthquake focal depths (in km) between 45° N and 49° N latitude as a function of longitude (decimal degrees) in Washington State, 1970–2006 (data from PNSN). Earthquakes occurring south of 47.25° N ($n = 2896$) are shown as gray dots, earthquakes north of 47.25° N ($n = 1463$) are shown as black dots. Downward triangle shows approximate longitude of the coast, solid bar shows the western and eastern limits of the Cascades, and triangles indicate position of the Quaternary volcanoes. Lower limit of earthquake foci for the North American plate is ~ 30 km.

the North American Plate is ~ 30 km ($D \sim 2.0 \times 10^{23}$ N m) in the Cascade region of Washington (Figure 4).

Using an entirely different technique, Lowry *et al.* (2000) use gravity anomaly and topographic data to model T_e for the entire Cordillera of the US. For the Cascade region of Washington, Lowry *et al.* (2000) calculate an average T_e of 26 ± 6.5 km ($D \sim 1.3 \times 10^{23}$ N m), with minimum and maximum constraints of 16 km and 40 km respectively ($D \sim 3.0 \times 10^{22}$ N m and 4.8×10^{23} N m). Of all the existing constraints on the rigidity of the crust in the Cascade region, only Lowry *et al.* (2000) indicate some spatial heterogeneity in T_e , with the region just south of the northern–southern Cascade boundary having on average a lower T_e (~ 20 km) than directly to the north of that boundary (~ 35 km). However, there is much overlap in T_e values between the northern and southern Cascades, and therefore we are comfortable assuming a homogeneous rigidity for the whole region in our model. Each of the different methods indicates a T_e between 25 and 40 km, equivalent to a D of ~ 1 to 5×10^{23} N m, a range of less than one order of magnitude.

Hillslope geometry

While isostatic compensation from valley incision increases peak altitudes and the relief above the mean, other hillslope geometry factors may also influence trends in ridge–valley relief and altitude in the Cascades. One possibility is that the northern Cascades are higher simply because the northern part of the range is wider than in the south. Another possible control on mean altitudes is the average hillslope length and slope of the area; on average, areas with long or steep hillslopes will have higher mean altitudes than areas with relatively shorter or gentler hillslopes. Hence, we may ask whether the North Cascades are higher simply because they have more widely spaced main drainages and/or steeper slopes than the southern Cascades in effect ‘prop up’ mean

altitudes. We thus tested for any systematic trends in trunk channel length and baselevel altitude, to assess whether the northern Cascades might rise to greater altitudes simply because the range is wider or the rivers cut to a higher baselevel. We also determined the extent to which observed north–south differences in mean altitudes are attributable to systematic variation in average hillslope lengths and slopes.

To test whether the northern Cascades are higher simply because the northern part of the range is wider, we compared the maximum channel length within each watershed between north and south. We used channel length rather than simply range width because, if concavity is consistent from north to south, longer streams should reach to higher altitudes. We used a GIS river coverage from the Washington State Department of Ecology (<http://www.ecy.wa.gov/services/gis/data/data.htm#rivers>), accessed in June 2008. The scale of this coverage is 1:100 000. For each watershed, we determined the channel length from the headwaters to where the stream exits the Cascade physiographic province, choosing the course that produced the longest channel length. For several of our watersheds (Snohomish, Stillaguamish, South Columbia), there are two or more exits because the main tributary confluences lie downstream of the Cascade Range boundary; in these situations, we chose the longest channel.

We calculated average hillslope lengths based on drainage density and using flow direction algorithms to calculate the mean downstream distance between ridges and the channel network. For both of these methods, we divided the range by major watershed boundaries rather than by swath. We defined drainage basins of each major river by identifying ‘pourpoints’ where they exit the Cascade physiographic province, and using standard GIS techniques to determine area that drains to each pourpoint (Figure 1C). We then calculated the maximum channel length in each basin and the centroid of each drainage basin to compare relative north–south positions (Figure 1C). Because drainage density and hillslope length are scale dependent, we defined two

resolutions of the channel network: cells with $\geq 1 \text{ km}^2$ of flow accumulation area and those with $\geq 10 \text{ km}^2$ of flow accumulation area. To calculate drainage density (D_d), we measured the length of channel per unit area for each watershed. The relationship between average hillslope length (l_s) and D_d is given by Horton (1945):

$$l_s = \frac{1}{2D_d} \quad (5)$$

The second method for determining hillslope lengths was to measure directly the distance between ridges (areas with accumulation area = 1 cell) and channels (accumulation area ≥ 1 and $\geq 10 \text{ km}^2$) as measured down the steepest descent (Figure 5A). We then calculated the mean and standard deviation of these distances within each watershed. The slope of each 10 m by 10 m grid cell was determined using the steepest descent angle defined by each cell's eight nearest neighbors. We then calculated the mean and standard deviation of slope for each drainage basin.

The slopes and the different measures of hillslope length were then used to quantify the extent to which differences in the mean altitude of each drainage basin are due to differences in mean hillslope length (\bar{l}_s) and mean slope ($\bar{\theta}$) (Figure 5). For each drainage basin, we used the following equation to determine mean altitude (\bar{Z}_m) above the local datum of the valley floor:

$$\bar{Z}_m = \frac{1}{2} \bar{l}_s \tan(\bar{\theta}) \quad (6)$$

We calculated ΔZ_m as the difference in \bar{Z}_m between each basin and the lowest \bar{Z}_m of all the basins. This ΔZ_m is the

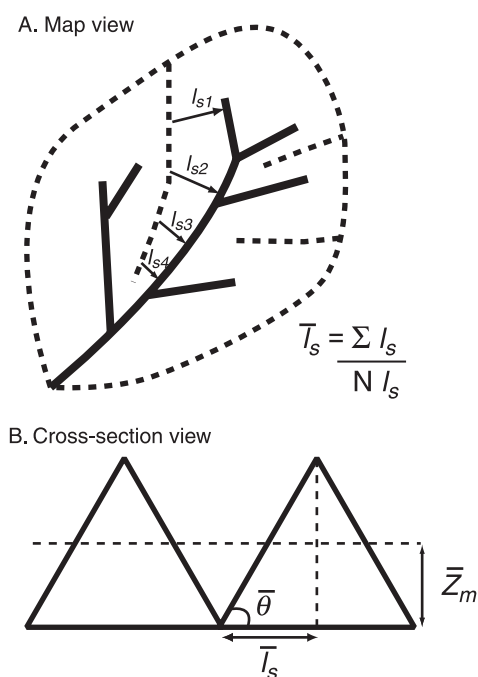


Figure 5. Diagrams of hillslope length (l_s) and mean altitude above the valley bottom (Z_m). (A) Map view of a hypothetical drainage basin; streams are solid bold lines, dashed lines are ridges (accumulation area = 1 cell). The first method for determining was to calculate the drainage density of each basin from stream length and basin area and use Equation 5 to calculate mean hillslope length. The second method was to find the average steepest downslope distance between ridges and streams (l_{s1} , l_{s2} , l_{s3} , l_{s4}). (B) Cross-section view of hypothetical drainage basin. Once the average hillslope length and slope of each basin was determined, we use Equation 6 to find the average relief above the valley bottoms for each basin.

degree to which the difference in measured mean north–south altitude could be attributable to the geomorphic parameters of slope and valley spacing.

Results

The northern Cascades are 'higher' than the southern Cascades in every measure. Mean altitudes in the Cascades range from $< 800 \text{ m}$ in southernmost swaths to $\sim 1300 \text{ m}$ in northernmost Washington (Figure 6A). Similarly, average maximum altitudes increase from $\sim 950 \text{ m}$ in the south to over 1800 m in the north (Figure 6A). The average altitude of the five highest peaks in each swath also increases to the north, ranging from $< 1800 \text{ m}$ in swaths 1–4, averaging $\sim 2200 \text{ m}$ in swaths 5–13, and averaging $\sim 2700 \text{ m}$ in the northernmost six swaths (14–19) (Figure 6A). Because the average maximum altitude increases at a steeper gradient towards the north than do the mean altitudes, the ARAMA increases from ~ 350 to 450 m in southern Washington to 550 to 750 m in the north (Figure 6B).

There is a greater amount of mass 'missing' between peaks in the northern part of the range, where deep valleys extensively dissect the high-altitude topography (Figure 7). As a result, there is greater potential for superelevation in the North Cascades than in the southern Cascades. As expected, both the magnitude of superelevation in a given area and the difference in superelevation between north and south are highly dependent on the flexural rigidity used in the calculation (Figure 8). The mean and maximum superelevations within each swath increase from south to north for all modeled flexural rigidities (Figure 9). For example, using the Airy endmember

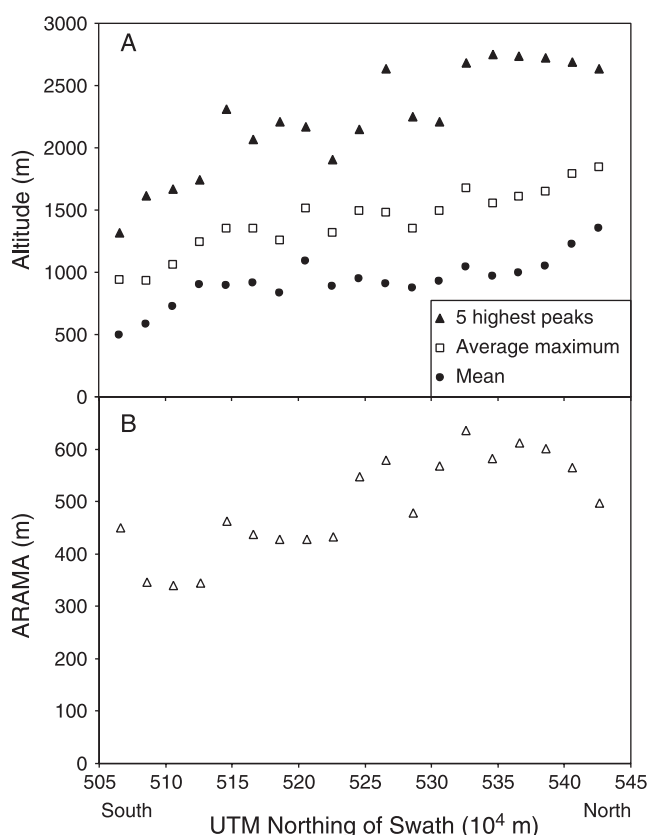


Figure 6. (A) Average altitude of the five highest non-volcanic summits (filled triangles), average altitude of the maximum topography profile (squares) and mean altitude (filled circles) in each swath shown in Figure 1. (B) Average relief above mean altitude (ARAMA), calculated by subtracting the mean altitude from the average maximum altitude in each swath.

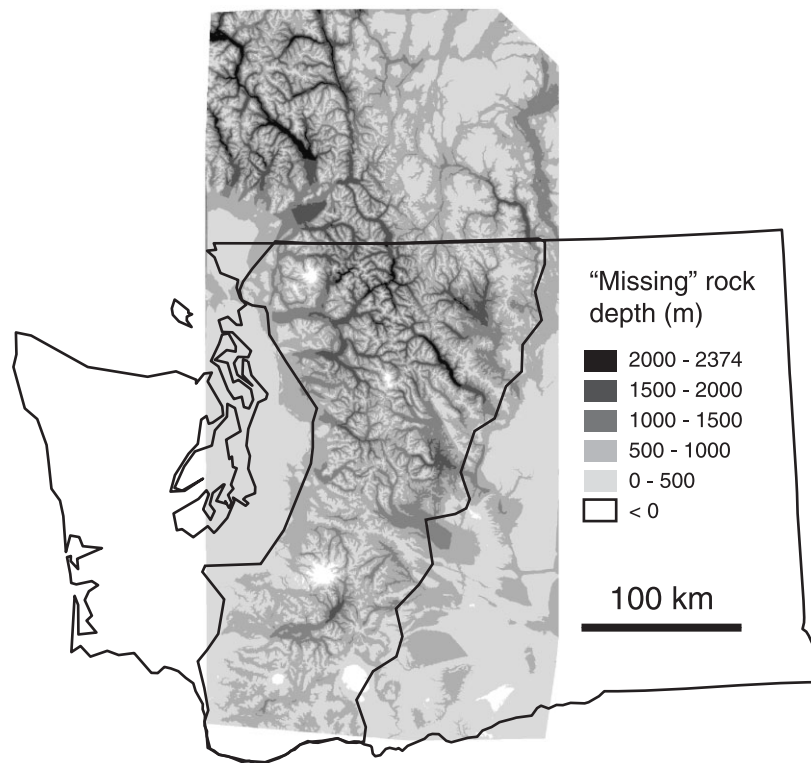


Figure 7. Depth of ‘missing’ rock in meters. Depths were calculated by subtracting the DEM from a hypothetical surface connecting peaks.

Table II. Mean superelevation and ARAMA in swaths

Swath	Swath UTM	ARAMA	Mean <i>w</i> (m)						<i>w</i> as percent of ARAMA						Maximum <i>w</i> (m)	
			10 ¹⁹ ^a	10 ²⁰	10 ²¹	10 ²²	10 ²³	10 ²⁴	10 ¹⁹	10 ²⁰	10 ²¹	10 ²²	10 ²³	10 ²⁴	10 ²³	10 ²⁴
1	5065965	450	160	169	167	187	165	86	36	37	37	41	37	19	172	90
2	5085975	346	397	344	281	247	182	89	115	99	81	71	52	26	238	118
3	5105985	340	384	378	364	334	229	107	113	111	107	98	67	32	301	146
4	5125995	344	388	398	431	417	284	133	113	115	125	121	83	39	357	172
5	5146005	462	620	595	552	490	335	158	134	129	120	106	72	34	404	196
6	5166015	438	630	605	561	505	358	172	144	138	128	115	82	39	436	213
7	5186025	428	466	479	504	513	382	186	109	112	118	120	89	44	469	229
8	5206035	428	559	548	555	575	433	212	131	128	130	134	101	49	497	241
9	5226045	433	698	678	652	633	468	228	161	157	151	146	108	53	521	250
10	5246055	547	697	701	704	671	487	236	127	128	129	123	89	43	550	263
11	5266065	579	841	807	770	726	524	253	145	139	133	125	91	44	584	282
12	5286075	478	800	785	765	742	546	265	167	164	160	155	114	56	617	300
13	5306085	568	774	758	754	751	560	274	136	134	133	132	99	48	651	318
14	5326095	635	830	815	796	777	573	278	131	128	125	122	90	44	681	331
15	5346105	582	873	848	833	798	579	280	150	146	143	137	99	48	703	340
16	5366115	612	887	870	852	805	578	278	145	142	139	132	94	45	712	343
17	5386125	601	916	879	837	794	574	277	152	146	139	132	95	46	713	343
18	5406135	565	791	787	791	780	575	279	140	139	140	138	102	49	709	341
19	5426145	496	779	759	754	753	562	275	157	153	152	152	113	55	704	340

^a Value of *D* in Nm.

(*D* = 10¹⁹ N m), the mean superelevations in the north and south are ~900 and 400 m respectively, contributing on average ~500 m more altitude to peaks in the north compared to the south.

However, limiting *D* to a regionally consistent value of 1 × 10²³ N m (*T_e* ~ 24 km) limits the mean superelevation to ~275 and 575 m in swaths 2–5 and 15–19 respectively. Considering the altitude of the highest peaks in those swaths, 1900 m and 2700 m, respectively, superelevation contributes to <25% of peak altitudes. Furthermore, the contribution of isostatic uplift

to the overall altitude difference between north and south is <300 m of the observed 800 m altitude difference (Table II).

The average relief above the mean increases towards the north, meaning that as more mass is missing in a swath relative to the peak altitudes, superelevation increases as well (Figure 9). What is intriguing, however, is that ARAMA is essentially equivalent to superelevation for the case where *D* = 1 × 10²³ N m, particularly for the northernmost swaths (Figure 9). This relationship may suggest that when *D* is properly constrained, superelevation (at least when averaged over a

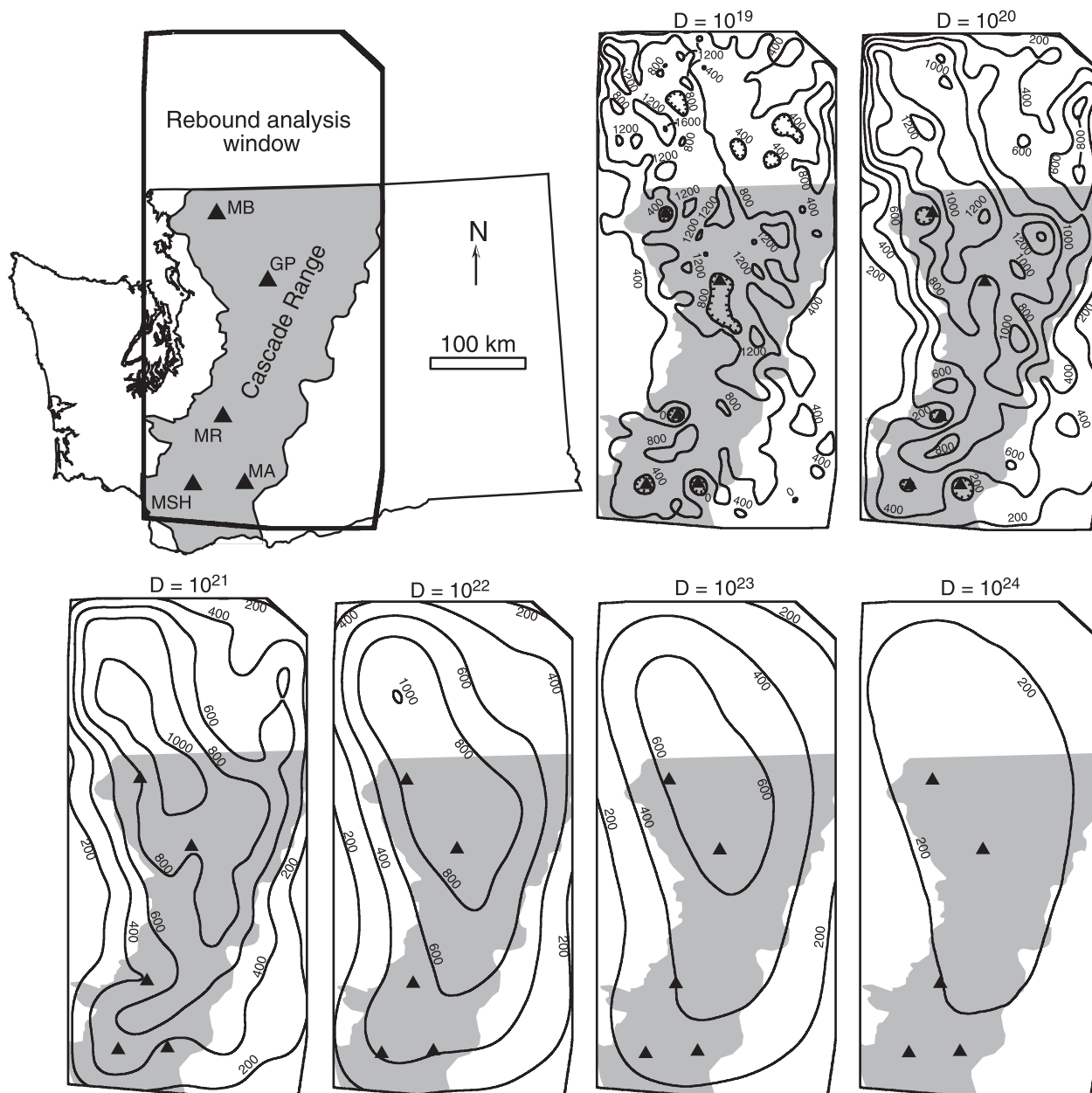


Figure 8. Contour maps of vertical deflection (superelevation) due to valley incision (w , see Equation 2). Upper left shows relationship between rebound analysis window, Cascade region, and Washington State borders. Quaternary volcanoes are indicated with filled triangles and Cascade region is shaded. The six panels represent superelevation (w from Equation 2) calculated using different flexural rigidities (D), noted above each panel. Note that the contour interval for $D = 10^{19}$ panel is 400 m; contour interval = 200 m for all other panels.

large area) should not generally exceed the average relief above the mean for that area. If true, the ARAMA for an area, which involves relatively simple GIS calculations, could provide an easier constraint on maximum superelevation than the much more computationally complex three-dimensional calculation of lithospheric deflection from unloading for a particular value or somehow constrained range of T_e values.

There are no consistent latitudinal trends in either baselevel (pourpoint) altitudes or maximum channel lengths for major Cascade watersheds. West-draining rivers generally exit the Cascades within 50 m of sea level along the entire north-south flank. East-draining rivers have pourpoints ranging from ~200 to 350 m, with the highest baselevels in the northern and southern ends of the range (Table III). There is also no systematic increase of maximum channel length towards the north; in other words, though the range is wider in the north, the rivers are not discernibly longer (Table III).

Mean hillslope lengths calculated from individual drainage basins using drainage density and mean downstream distances

from ridges to streams are similar for most basins, ranging from ~550 to 900 m using the 1 km² stream network and ~1900–2500 m using the 10 km² stream network (Table III, Figure 10A). The method used to determine hillslope length has a slight effect on the trends; mean hillslope lengths tend to be somewhat longer using the downslope method than the drainage density method, particularly in southern drainages. As a result, mean hillslope lengths increase slightly towards the north when determined using drainage density; however, hillslope lengths do not have much latitude dependence when determined using the downslope distance calculation.

In contrast, mean slope angles are 11° to 22° in the southern half of the range and increase to 20°–27° in the northern half, although standard deviations for all overlap (Figure 10B). As a result, the calculated mean altitude above the valley floor based on mean slope angles is higher in the northern basins than in the southern basins (Figure 11). The modeled mean altitudes from the 1 km² stream network are at most 135 m higher in the north than south. The mean altitude above the

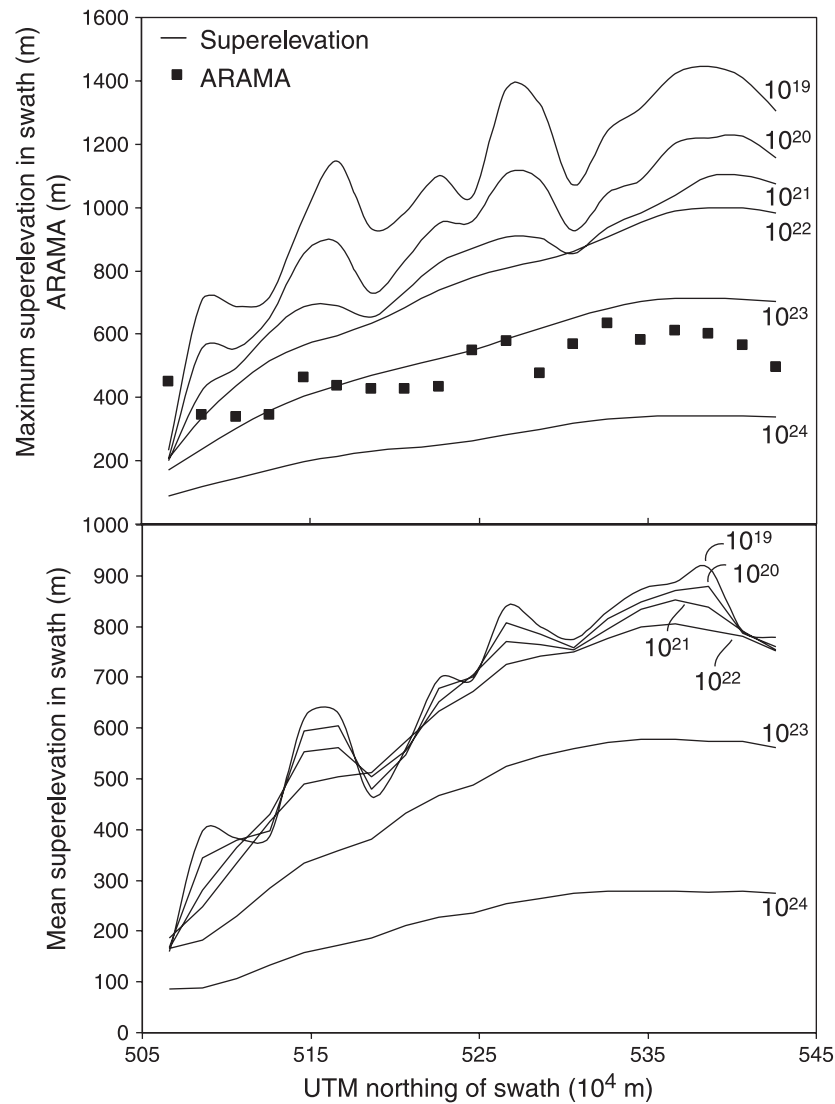


Figure 9. Maximum (top panel) and mean (bottom panel) superlevation in each swath (Figure 1) for flexural rigidities of $D = 1019, 1020, 1021, 1022, 1023,$ and 1024 N m. Filled squares in top panel show ARAMA for each swath.

Table III. Drainage basin characteristics

Drainage basin	UTM northing of drainage centroid (m)	Basin area ^a (km ²)	Maximum channel length (km)	Mean $\pm 1\sigma$ slope (deg)	Pourpoint altitude (m)	Mean altitude (m)	Basin relief (m)	Drainage density (10 ⁻⁴ m)	Drainage density 10 km ² (10 ⁻⁴ m)
Similkameen	5464591	1572.1	NA	19.51 \pm 10.84	349	1570	2310	6.954	2.387
Nooksack	5406495	1620.6	93	21.43 \pm 12.48	21	839	3262	7.133	2.504
Skagit	5385139	6969.7	170	26.93 \pm 14.09	5	1094	3277	6.460	2.427
Methow	5378138	4712.3	162	22.23 \pm 11.35	237	1416	2487	6.702	3.717
Stillaguamish	5341494	1156.4	66	20.90 \pm 13.74	31	691	2058	6.959	2.516
Chelan	5340391	2413.0	134	27.21 \pm 13.61	216	1346	2677	6.579	2.410
Entiat	5304868	1082.7	89	23.97 \pm 10.52	216	1288	2603	7.018	2.327
Wenatchee	5286537	3440.0	140	25.20 \pm 12.16	190	1200	2678	6.640	2.464
Snohomish	5284847	3518.7	94	26.38 \pm 13.49	0.2	827	2428	6.873	2.540
Cedar-Green	5236433	903.4	61	22.00 \pm 11.07	238	860	1510	6.676	2.254
Yakima	5217881	5538.6	137	17.45 \pm 11.64	329	966	2100	8.382	2.545
Puyallup	5207331	2020.2	73	21.88 \pm 12.64	61	1070	4332	7.225	2.009
Naches	5183251	2861.8	113	19.07 \pm 11.09	329	1249	2167	7.262	2.530
Nisqually	5180140	1155.1	73	17.88 \pm 11.89	137	816	4256	7.513	2.921
Cowlitz	5145060	5702.1	218	18.74 \pm 12.15	3	778	4263	7.194	2.624
Klickitat	5099823	3500.4	149	11.73 \pm 9.56	23	912	3725	8.532	2.736
Lewis	5096477	2691.6	163	15.72 \pm 11.11	0.6	682	3666	7.605	2.535
South Columbia	5080864	2346.7	67	14.77 \pm 10.87	20	786	3725	7.639	2.543

^a Within analysis area.

Note: NA, not available.

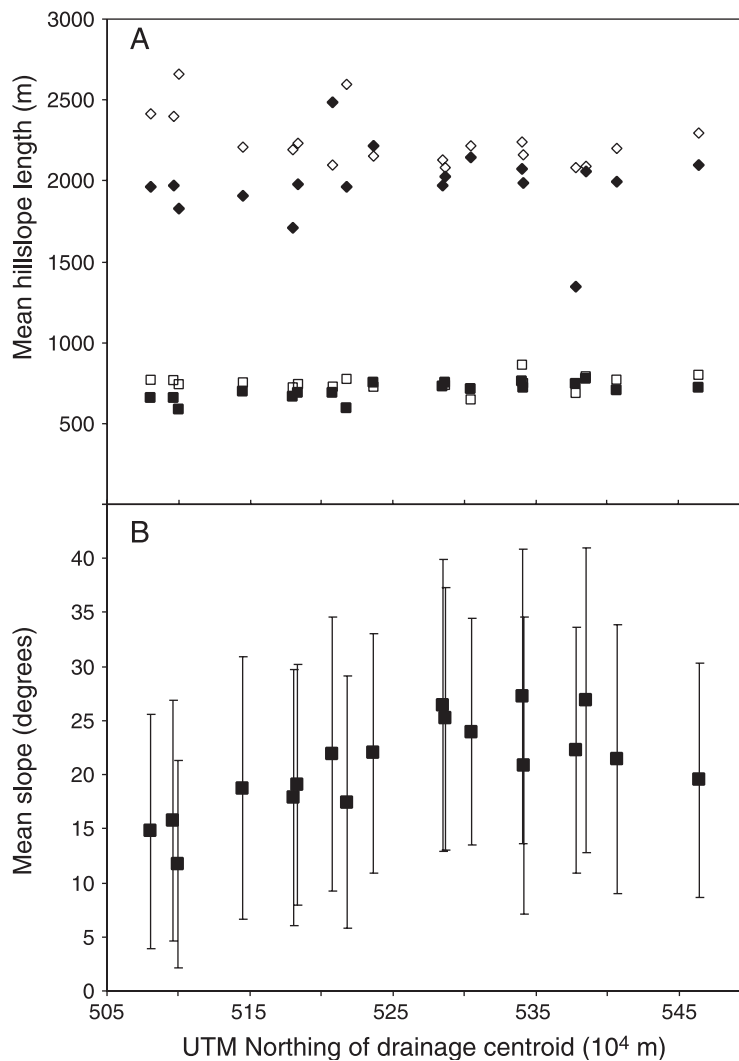


Figure 10. (A) Mean hillslope lengths calculated for drainage basins (Figure 1C). Diamond symbols represent values calculated from 10 km² accumulation area: open diamonds = downslope method, filled diamonds = drainage density method. Square symbols represent values calculated from 1 km² accumulation area: open squares = downslope method, filled squares = drainage density method. (B) Mean slope angle of all cells in each basin; error bars are one standard deviation from the mean.

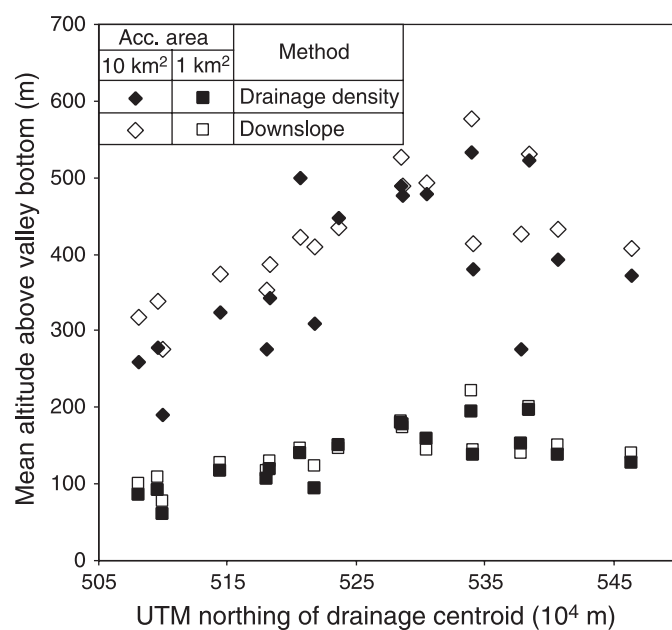


Figure 11. Modeled mean altitude above valley bottoms for Cascade drainage basins (Figure 1C, Table III). Diamond symbols represent values calculated from 10 km² accumulation area: open diamonds = downslope method, filled diamonds = drainage density method. Square symbols represent values calculated from 1 km² accumulation area: open squares = downslope method, filled squares = drainage density method.

valley floor using the 10 km² stream network is about 350 m higher in the north than in the south (Figure 11).

Discussion

Using a conservative constraint of D (1×10^{23} N m) we determine the maximum possible superelevation and thus additional peak altitude that could have been created in the Cascades as a result of valley incision. The maximum possible superelevation that can be achieved at a single spot in the Cascades is 700 m in the northern region (Table II, Figure 9). When averaged over swaths, the upper limit on average superelevation ranges from 575 m in the North Cascades to <300 m in the southern Cascades. This amount of superelevation represents <25% of the observed highest summit altitudes. However, many of these valleys must have existed prior to glaciation, and erosion from valley glaciers has been suggested to about double the cross-sectional area, and thus volume, of pre-glacial valleys in the Pacific Northwest (Montgomery, 2002; Amerson *et al.*, 2008). Assuming a similar ratio of glaciated to unglaciated valley geometry in the Cascades, the effect of global cooling, the onset of glaciation, and the glacial excavation of pre-existing fluvial valleys likely accounted for only half the overall superelevation measured by our model. Therefore, glacial erosion alone likely increased the highest summit altitudes by at most only 350 m, insufficient to create a new orographic barrier from a low- or modest-altitude landscape or trigger a large-scale change in regional climate.

Differential incision of the Cascades contributes only modestly to the overall altitude difference between the northern and southern parts of the range. Based on our constraints of D , the largest difference between maximum and mean superelevation between northern and southern regions is ~500 and 300 m, respectively. However, the highest peaks in the northern Cascades are ~1000 m higher than those in southern Washington, and the average maximum altitudes are ~800 m higher in the north than south. Assuming the largest possible effect (incision of valleys beneath the peak 'surface'), differences in incision between north and south can account for only about half of the total difference in the altitude of the peaks. If we assume that fluvial valleys predated the existing glacial valleys, the effect of glacial excavation alone accounts for significantly less of the difference. In addition, while average ridge-to-valley lengths are relatively constant between north and south, the generally higher slopes in the North Cascades give that region average altitudes about 350 m farther above the valley floors than in the south (Figure 10). Again, while this effect is measurable, it cannot account for the remaining difference in either mean or maximum altitudes between the northern and southern Cascades. Finally, the northern Cascades are not higher simply because the range is wider there, as there is no systematic increase in fluvial channel length toward the north.

We conclude that tectonic, geologic, or geophysical distinctions, such as differences in rock uplift rate, crustal thickness, mantle temperature, etc., must contribute to the higher altitudes in the Cascades of northern Washington. This result is consistent with the interpretation first presented by Mackin and Cary (1965) and recently supported by Mitchell and Montgomery (2006a) that the northern and southern Cascade Range in Washington had strikingly different geologic, tectonic, and geomorphic histories since the Miocene. For example, Mitchell and Montgomery (2006a) show that the Cascades in northern Washington were quite high since before the initial eruption of the 15 My-old Columbia River Basalts, and that the crystalline core of the northern part of the range may

be acting as a relatively immobile, rigid tectonic barrier. Conversely, the Cascades of southern Washington were relatively low until after the eruption of the basalts, whereupon they rose to their current altitude likely due to north–south compression.

Conclusions

Using plausible crustal strength constraints, the maximum possible superelevation of the Cascade Range due to isostatic response from valley incision is 700 m, with an average superelevation of 575 m in the north and 300 m in the south. In the Cascades, the average amount of superelevation is comparable to the average relief above the mean in that same area. The overall magnitude of uplift is consistent with analyses from prior studies in other regions; <25% of the altitudes of the highest peaks in their respective areas. As glacial erosion likely accounts for only about half of that superelevation, glacial widening and deepening of valleys is not responsible for changing atmospheric conditions, such as creating the Cascade Range rainshadow.

Peak uplift due to isostatic effects from valley incision accounts for <300 m of the difference in peak altitudes between the northern and southern Cascades. Because peak altitudes are 800–1000 m higher in the northern than southern Cascades (Figure 6), some other factor must be responsible for the remaining 500–700 difference. The relief created by overall steeper slopes in the Cascades of northern Washington is responsible for propping mean altitudes above valley bottoms up to 350 m higher than those in southern Washington. While these parameters are not directly comparable, mean altitudes are up to 1000 m higher in the northern Cascades than in the southern Cascades. Therefore, several hundred meters of the difference in mean and maximum altitudes between the northern and southern Cascades in Washington must be due to geologic or tectonic differences between the two regions, a conclusion consistent with previous interpretations regarding the topographic histories of the two regions (e.g. Mackin and Cary, 1965; Mitchell and Montgomery, 2006a).

Acknowledgements—This research was funded by National Science Foundation (NSF) research grant EAR-0087413 and an NSF Graduate Research Fellowship, the Department of Earth and Space Sciences at the University of Washington, and a Batchelor (Ford) Foundation grant from the College of the Holy Cross. Comments on early drafts from S. C. Porter, J. O. Stone, the late R. J. Stewart, and reviews from S. Brocklehurst and anonymous reviewers greatly improved this manuscript.

References

- Abramowitz M, Stegun IA. 1964. *Handbook of Mathematical Functions*. Dover Publications: New York.
- Amerson BE, Montgomery DR, Meyer G. 2008. Relative size of fluvial and glaciated valleys in central Idaho. *Geomorphology* **93**: 537–547.
- Burov EB, Watts AB. 2006. The long-term strength of the continental lithosphere: 'jelly sandwich' or 'crème brûlée'? *GSA Today* **16**: 4–10. DOI: 10.1130/1052-5173(2006)016<4:TLTSC>2.0.CO;2
- Clague JJ, James TS. 2002. History and isostatic effects of the last ice sheet in southern British Columbia. *Quaternary Science Reviews* **21**: 71–87.
- Cohen SC, Darby DJ. 2003. Tectonic plate coupling and elastic thickness derived from the inversion of a steady state viscoelastic model using geodetic data: application to southern North Island, New Zealand. *Journal of Geophysical Research* **108**: 2164. DOI: 10.1029/2001JB001687

- England PC, Wells RE. 1991. Neogene rotations and quasicontinuous deformation of the Pacific Northwest continental margin. *Geology* **19**: 978–981.
- Flück P, Hyndman RD, Lowe C. 2003. Effective elastic thickness T_e of the lithosphere in western Canada. *Journal of Geophysical Research* **108**: 2430. DOI: 10.1029/2002JB002201
- Gilchrist AR, Summerfield MA, Cockburn HAP. 1994. Landscape dissection, isostatic uplift, and the morphologic development of orogens. *Geology* **22**: 963–966.
- Hasterok D, Chapman DS. 2007. Continental thermal isostasy: 2. Application to North America. *Journal of Geophysical Research* **112**: B06415. DOI: 10.1029/2006JB004664
- Haugerud RA. 2004. *Cascadia – Physiography: USGS Miscellaneous Investigations Map I-2689*. USGS: Renton, VA.
- Hermann RB. 1979. FASTHYPO: a hypocenter location program. *Earthquake Notes* **50**(2): 25–37.
- Holmes A. 1945. *Principles of Physical Geology*. Thomas Nelson and Sons: London.
- Horton RE. 1945. Erosional development of streams and their drainage basins, hydrophysical approach to quantitative morphology. *Geological Society of America Bulletin* **56**: 275–370.
- James TS, Clague JJ, Wang K, Hutchinson I. 2000. Postglacial rebound at the northern Cascadia subduction zone. *Quaternary Science Reviews* **19**: 1527–1541.
- Lambeck K. 1988. *Geophysical Geodesy: The Slow Deformation of the Earth*. Clarendon Press: Oxford.
- Lowry AR, Ribe NM, Smith RB. 2000. Dynamic elevation of the Cordillera, western United States. *Journal of Geophysical Research* **105**: 23372–23390.
- Mackin JH, Cary AS. 1965. Origin of Cascade landscapes. *Washington Division of Mines and Geology Information Circular* **41**: 35.
- Maggi A, Jackson JA, McKenzie D, Priestley K. 2000. Earthquake focal depths, effective elastic thickness, and the strength of the continental lithosphere. *Geology* **28**: 485–498.
- Medvedev S, Hartz EH, Podladchikov YY. 2008. Vertical motions of the fjord regions of central East Greenland: impact of glacial erosion, deposition, and isostasy. *Geology* **36**: 539–542.
- Miller RB, Paterson SR. 2001. Influence of lithological heterogeneity, mechanical anisotropy, and magmatism on the rheology of an arc, North Cascades, Washington. *Tectonophysics* **342**: 351–370.
- Mitchell SG, Montgomery DR. 2006a. Polygenetic topography of the Cascade Range, Washington State, USA. *American Journal of Science* **306**: 736–768.
- Mitchell SG, Montgomery DR. 2006b. Influence of a glacial buzzsaw on the height and morphology of the Cascade Range in central Washington State, USA. *Quaternary Research* **65**: 96–107.
- Molnar P, England PC. 1990. Late Cenozoic uplift of mountain peaks: chicken or egg? *Nature* **346**: 29–34.
- Montgomery DR. 1994. Valley incision and the uplift of mountain peaks. *Journal of Geophysical Research* **99**: 13913–13921.
- Montgomery DR. 2002. Valley formation by fluvial and glacial erosion. *Geology* **30**: 1047–1050.
- Montgomery DR, Greenberg HM. 2000. Local relief and the height of Mt. Olympus. *Earth Surface Processes and Landforms* **25**: 385–396.
- Pelletier JD. 2004. Estimate of three-dimensional flexural-isostatic response to unloading: rock uplift due to late Cenozoic glacial erosion in the western United States. *Geology* **32**: 161–164.
- Perez-Gussinye M, Lowry AR, Watts AB, Velicogna I. 2004. On the recovery of effective elastic thickness using spectral methods: examples from synthetic data and from the Fennoscandian Shield. *Journal of Geophysical Research* **109**: B10409. DOI: 10.1029/2003JB002788
- Schuster JE. 2005. *Geologic map of Washington State*, Washington Division of Geology and Earth Resources GM 53, 1 sheet, scale 1: 500 000, 44 pp. text. Washington Department of Natural Resources: Olympia, WA.
- Small EE, Anderson RS. 1998. Pleistocene relief production in Laramide mountain ranges, western United States. *Geology* **26**: 123–126.
- Stern TA, Baxter AK, Barrett PJ. 2005. Isostatic rebound due to glacial erosion within the Transantarctic Mountains. *Geology* **33**: 221–224.
- Thatcher W, Pollitz FF. 2008. Temporal evolution of continental lithospheric strength in actively deforming regions. *GSA Today* **18**: 4–11.
- Turcotte DL, Schubert G. 1982. *Geodynamics: Applications of Continuum Physics to Geological Problems*. Wiley: New York.
- Wager LR. 1933. The rise of the Himalaya. *Nature* **132**: 28.
- Watts AB. 2001. *Isostasy and Flexure of the Lithosphere*. Cambridge University Press: Cambridge.
- Watts AB, Burov EB. 2003. Lithospheric strength and its relationship to the elastic and seismogenic layer thickness. *Earth and Planetary Science Letters* **213**: 113–131.
- Whipple KX, Kirby E, Brocklehurst SH. 1999. Geomorphic limits to climatically induced increases in topographic relief. *Nature* **401**: 39–43.